Low-loss light coupling with graded-index core polymer optical waveguides via 45-degree mirrors

Yoshie Morimoto[1,*] and Takaaki Ishigure[2]

[1] *Graduate School of Science and Technology, Keio University, 3-14-1 Hiyoshi, Kohoku-ku, Yokohama, 223-8522, Japan*

[2] *Faculty of Science and Technology, Keio University, 3-14-1 Hiyoshi, Kohoku-ku, Yokohama, 223-8522, Japan*

[*] *y.mo-ri@keio.jp*

Abstract: We experimentally investigate the optical loss of graded-index (GI) core polymer optical waveguides with a 45-degree mirror on their one end fabricated using the photo-addressing method. In addition, we also theoretically analyze the loss of GI square-core waveguides with mirrors using a ray-trace simulation tool. Then, in the waveguide based optical link including the optical path conversions via 45-degree mirrors, we show that GI waveguides realize lower total optical loss than conventional step-index (SI) core waveguides. The lower loss in the GI waveguide link is attributed to the tight optical confinement at the core center even after reflection at the mirrors.

OCIS codes: (130.5460) Polymer waveguides; (200.4650) Optical interconnects; (230.4040) Mirrors; (080.5692) Ray trajectories in inhomogeneous media.

References and links

1. http://www/top500.org/
2. A. Benner, "Optical interconnect opportunities in super computers and high end computing," in *Optical Fiber Communication Conference and Exposition* (2012), paper Otu2B4.
3. R. Selvaraj, H. T. Lin, and J. F. Mcdonald, "Integrated optical waveguides in polyimide for wafer scale integration," J. Lightwave Technol. **6**(6), 1034–1044 (1988).
4. K. W. Jelley, G. T. Valliath, and J. W. Stafford, "High-speed chip-to-chip optical interconnect," IEEE Photonics Technol. Lett. **4**(10), 1157–1159 (1992).
5. G. L. Bona, B. J. Offrein, U. Bapst, C. Berger, R. Beyeler, R. Budd, R. Dangel, L. Dellmann, and F. Horst, "Characterization of parallel optical-interconnect waveguides integrated on a printed circuit board," Proc. SPIE **5453**, 134–141 (2004).
6. R. Dangel, C. Berger, R. É. Beyeler, L. Dellmann, M. Gmur, R. É. Hamelin, F. Horst, T. Lamprecht, T. Morf, S. Oggioni, M. Spreafico, and B. J. Offrein, "Polymer-waveguide-based board-level optical interconnect technology for Datacom application," IEEE Trans. Adv. Packag. **31**(4), 759–767 (2008).
7. R. C. A. Pitwon, K. Wang, J. Graham-Jones, I. Papakonstantinou, H. Baghsiahi, B. J. Offrein, R. Dangel, D. Milward, and D. R. Selviah, "FirstLight: pluggable optical interconnect technologies for polymeric electro-optical printed circuit boards in data centers," J. Lightwave Technol. **30**(21), 3316–3329 (2012).
8. Y. Takeyoshi and T. Ishigure, "High-density 2×4 channel polymer optical waveguide with graded-index circular cores," J. Lightwave Technol. **27**(14), 2852–2861 (2009).
9. T. Kosugi and T. Ishigure, "Polymer parallel optical waveguide with graded-index rectangular cores and its dispersion analysis," Opt. Express **17**(18), 15959–15968 (2009).
10. K. Soma and T. Ishigure, "Fabrication of a graded-Index circular-core polymer parallel optical waveguide using a microdispenser for a high-density optical printed circuit board," IEEE J. Sel. Top. Quantum Electron. **19**(2), 3600310 (2013).
11. R. Kinoshita, K. Moriya, K. Choki, and T. Ishigure, "Polymer optical waveguides with GI and W-shaped cores for high bandwidth density on-board interconnects," J. Lightwave Technol. **31**(24), 4004–4015 (2013).
12. T. G. Lim, P. V. Ramana, B. S. P. Lee, T. Shioda, H. Kuruveettil, J. Li, K. Suzuki, K. Fujita, K. Yamada, D. Pinjala, and J. L. H. Shing, "Demonstration of direct coupled optical/electrical circuit board," IEEE Trans. Adv. Packag. **32**(2), 509–516 (2009).
13. T. Mori, K. Takahama, M. Fujiwara, K. Watanabe, H. Owari, Y. Shirato, S. Terada, M. Sakamoto, and K. Choki, "Optical and electrical hybrid flexible printed circuit boards with unique photo-defined polymer waveguide layers," Proc. SPIE **7607**, 76070S (2010).
14. Y. Morimoto, R. Kinoshita, A. Takahashi, and T. Ishigure, "45-degree mirrors on graded-index core polymer optical waveguides for low-loss light coupling," in *Proc. IEEE Photonics Conference* (IEEE, 2014), pp. 48–49.

#255734 Received 14 Dec 2015; revised 30 Jan 2016; accepted 1 Feb 2016; published 11 Feb 2016

15. T. Ishigure, K. Shitanda, and Y. Oizmi, "Index-profile design for low-loss crossed multimode waveguide for optical printed circuit board," Opt. Express **23**(17), 22262–22273 (2015).
16. T. Mori, K. Moriya, K. Kitazoe, S. Takayama, S. Terada, M. Fujiwara, K. Takahama, K. Choki, and T. Ishigure, "Polymer optical waveguide having unique refractive index profiles for ultra high-density interconnection," in *Optical Fiber Communication Conference and Exposition 2012* (OSA, 2012), paper Otu1L6.

1. Introduction

Over the last decades, the arithmetic capacity of high performance computers (HPCs) has grown explosively [1]. To keep increasing the HPC performance, high bandwidth density data exchange is required in their racks and even on boards maintaining the low power consumption. Hence, optical interconnect technologies have been drawing much attention. In fact, multimode fiber (MMF) links have already been deployed as board-to-board interconnects in some current HPCs and datacenter networks, and the next issue is how to realize on-board optical interconnects [2]. Multimode polymer parallel optical waveguides have been regarded as one of the solutions. Actually, intensive efforts have been made on developing step-index (SI) polymer waveguides over the last thirty years [3–7].

Meanwhile, we have focused on graded-index (GI) core polymer waveguides, and experimentally demonstrated the superior properties of GI-core waveguides such as low propagation loss and high coupling efficiency with MMFs and photo detectors (PDs) because of the strong optical confinement effect of GI cores [8–10]. We already presented one of the promising fabrication methods for GI-core polymer optical waveguides named "Photo-addressing method," which was developed at Sumitomo Bakelite Co., Ltd. and demonstrated the low propagation loss and low coupling loss with an MMF even for square-shaped GI-cores [11]. However, these results were obtained when the waveguide core was perfectly aligned with light sources or photodiodes.

Meanwhile, in the actual application to optical-printed circuit boards (O-PCBs), the light source could be vertical cavity surface emitting lasers (VCSELs), which would be mounted on board along with photodiodes, and the signal light is coupled to and from the polymer waveguides via 45-degree mirrors fabricated on their ends [12]. Here, in order to apply the GI-core waveguides to the actual O-PCBs, the optical loss at the 45-degree mirrors is a concern.

Therefore, in this paper, we fabricate polymer optical waveguides which have 45-degree mirrors on one end, and investigate the optical properties of GI-core waveguides with a 45-degree mirror.

2. Optical link on O-PCBs

In this paper, we focus on both intra- and inter- board optical link composed of a pair of multimode polymer optical waveguides, as shown in Fig. 1. The light from a VCSEL chip mounted on the surface of the first O-PCB is coupled to the first waveguide integrated on the board via a 45-degree mirror on one end (intra-board). Then, the first and the second waveguides are connected with an MMF ribbon (inter-board). The second waveguide is connected to a photodetector (PD) mounted on the second O-PCB.

At the connection between a VCSEL/PD and waveguide, an optical path conversion via 45-degree mirrors is required as shown in Fig. 2. In this paper, we focus on the optical link including the optical coupling via 45-degree mirrors, and investigate the loss at the mirrors in detail.

#255734 Received 14 Dec 2015; revised 30 Jan 2016; accepted 1 Feb 2016; published 11 Feb 2016

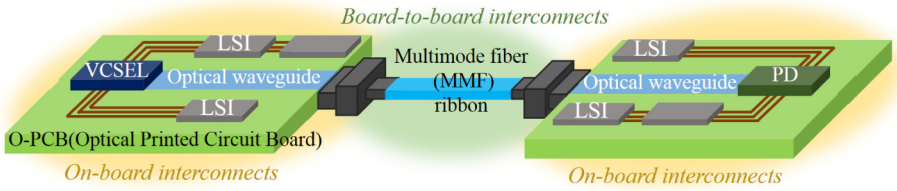

Fig. 1. On-board and board-to-board optical link.

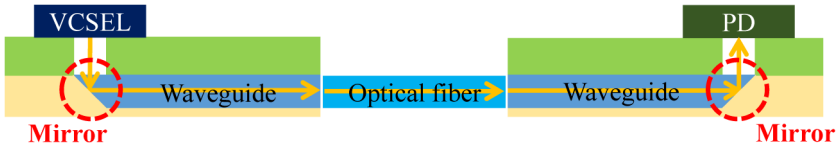

Fig. 2. Optical path conversion via a 45-degree mirror.

3. Fabrication for GI-core polymer optical waveguides: photo-addressing method

3.1 Photo-addressing method [13]

A fabrication process named the photo-addressing method is illustrated in Fig. 3. In the photo-addressing method, a polynorbornene resin is used. Its refractive index is varied by the UV intensity pattern illuminated during its curing, so just one monomer layer is sufficient for forming a waveguide structure.

First, a polynorbornene monomer including refractive index modifier is cast onto a substrate. Next, the coated monomer layer is exposed to UV light through a photo-mask to obtain the waveguide structure. After the UV exposure, post-baking is carried out to cure the monomer. Here, the UV-illuminated areas are cured prior to the masked areas to have a lower refractive index (n = 1.536), corresponding to the waveguide cladding section. On the other hand, the monomer diffuses from the masked areas to the illuminated areas to supplement the volume contraction due to curing.

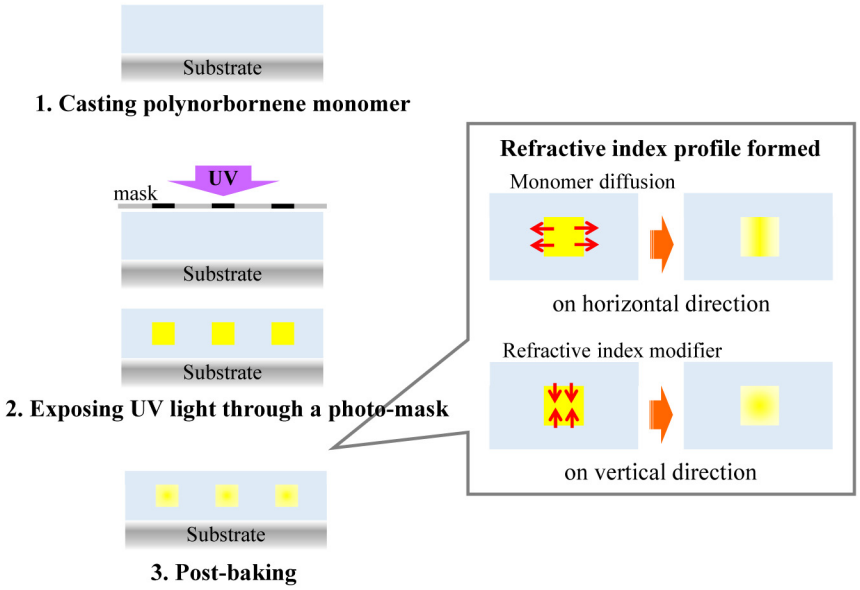

Fig. 3. Fabrication technique of the photo-addressing method.

#255734 Received 14 Dec 2015; revised 30 Jan 2016; accepted 1 Feb 2016; published 11 Feb 2016

Hence, the masked areas exhibit a high refractive index (n = 1.553) with a gradual variation at the core-cladding boundary, resulting in a parabolic index profile in the horizontal direction. Meanwhile, the refractive index modifier originally doped with the monomer plays a key role for the refractive index profile in the vertical direction. Thus, GI square core waveguides are fabricated using the photo-addressing method. In this paper, we focus on a GI square-core waveguide fabricated using this method.

3.2 Structure of the polymer waveguide

We characterize the GI-square core waveguides fabricated using the photo-addressing method and compared with a conventional SI-square core waveguide with the same core size. The SI and the GI waveguide are fabricated using the same kind of materials. A cross section of the GI square-core waveguide is shown in Fig. 4. The waveguide has a core size of 40 × 40 μm with a 62.5-μm inter-core pitch. The length of the waveguide is about 10 cm.

Figure 5 shows an over view of a 45-degree mirror section. The mirrors are fabricated by laser ablation using an excimer laser at 193-nm wavelength. One in every four cores has a mirror on its one end, so the mirror channels are aligned with a 250-μm pitch. In the following section, we investigate the optical loss of the waveguide: the averaged value of 6 channels with mirrors are compared.

Fig. 4. Cross section of a GI square-core waveguide.

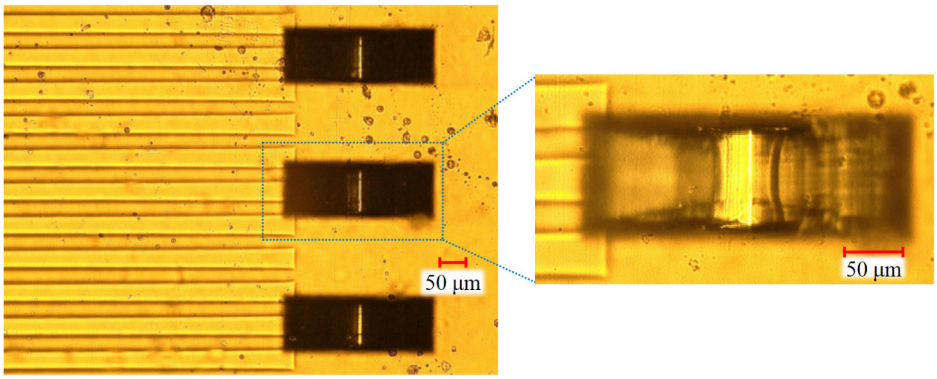

Fig. 5. Over view of a GI square-core waveguide with mirrors.

4. Characterization for square-core polymer waveguides

4.1 Measurement setup

Figure 6 shows the measurement setup for the loss of 45-degree mirrors implementing the optical link shown in Fig. 2 [14]. In this paper, we would like to investigate the loss difference between the Tx and Rx sides when the same mirror is used in the optical link shown in Fig. 2. However, it would be difficult to use two waveguides with completely identical characteristics (mirror angle, mirror surface roughness, etc.). Therefore, in the actual measurement, the measurement setup is divided into two, Tx side and Rx side, and just one waveguide with a mirror is used for the both measurements. Here, the waveguides in Figs. 6(a) and 6(b) are named “waveguide on the Tx side” and “waveguide on the Rx side,” respectively. With an LED source at 850-nm wavelength, we use a 1-m long single-mode

#255734 Received 14 Dec 2015; revised 30 Jan 2016; accepted 1 Feb 2016; published 11 Feb 2016

fiber (SMF) as a launch probe. This launch condition is provided as an alternative to a VCSEL chip with a spot size as small as 10-µm, although the wavelength spectrum is much broader. It is already experimentally verified that the wide wavelength spectrum of the LED exhibits negligible effects on the insertion loss, compared with VCSEL source, because the waveguide length is as short as 10 cm. The light from the SMF is coupled to the waveguide on the Tx side via a 45-degree mirror. Because the two waveguides are supposed to be connected by a 50-µmø GI-MMF, the other end of the waveguide on the Tx side is connected to a 1-m long 50-µmø GI-MMF in order to guide the output to an optical power meter.

Meanwhile, as mentioned earlier, the same waveguide with a mirror as Fig. 6(a) is used for the waveguide on the Rx side in Fig. 6(b), where the waveguide is excited using the same GI-MMF as the one in Fig. 6(a). In this measurement, a VCSEL source is used, by which a restricted mode launch (RML) condition is realized for the GI-MMF. In the actual link application shown in Fig. 2, the MMF should be excited under an RML condition for achieving a data rate of 10 Gbps and beyond. We confirmed that the near-field pattern (NFP) from the MMF probe connected to the VCSEL source satisfied the encircled flux (EF) requirements of International Electrotechnical Commission (IEC) 61280-4-1. The light propagating in the waveguide and reflected at the mirror is coupled to a 50-µmø SI-MMF as a substituent for a 50-µmø PD. Although a 50-µmø SI-MMF with higher NA than the waveguide is used, all the output light from the mirror is not necessarily coupled to the SI-MMF. Therefore, the loss observed in Fig. 6(b) could be higher than the loss in the actual link configuration. In these setups, the input and output connection points in the waveguides on the Tx and Rx sides are numbered as connection point 1 to 4 in order, as shown in Fig. 6.

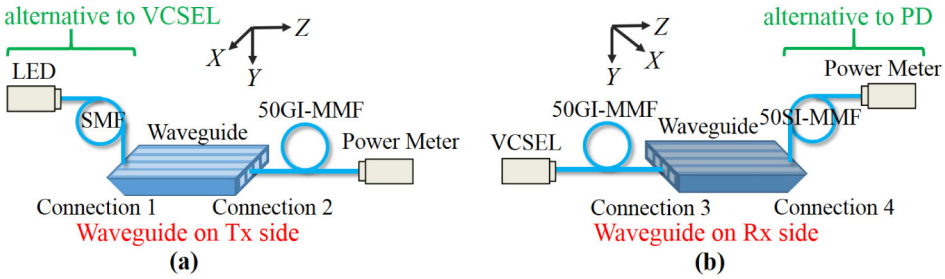

Fig. 6. Actual measurement setup on the (a) Tx side (b) Rx side.

4.2 Insertion loss

Table 1 summarizes the insertion loss of the SI and GI waveguides due to the 45° mirror, in which the difference of total insertion loss between the SI and GI waveguides is also shown. From Table 1, it is found that the insertion loss of the GI waveguide is lower than that of the SI waveguide at both the Tx and Rx sides, and the total loss of both sides is 4.18 dB in the GI waveguide, while it is 5.23 dB in the SI waveguide: 1.05-dB advantage in the GI-core waveguide is observed over the SI counterpart in the complete link.

This low-loss in the GI waveguide is attributed to the strong optical confinement effect of the GI-core. The NFPs measured at connection point 2 are shown in Fig. 7. For comparison, an NFP of the SMF probe with a mode-field diameter of 9 µm is shown in Fig. 8.

In the SI-core waveguide, the light intensity distribution from the waveguide is spread in the entire core even though it is launched with a quite small spot size. Hence, high coupling loss is caused at connection points 2 and 4, because of the core shape difference between the waveguide and MMFs (square and circle), corresponding to the mode-field mismatch. Contrastingly, the GI waveguide maintains the small spot size at its input end even after the mirror reflection as shown in Fig. 7 (b). This strong optical confinement effect of the GI core leads to a high coupling efficiency with the GI- and SI-MMFs at connection points 2 and 4, respectively, resulting in the low total link loss.

#255734 Received 14 Dec 2015; revised 30 Jan 2016; accepted 1 Feb 2016; published 11 Feb 2016

Thus, the total losses are experimentally confirmed to be less in the GI waveguide link than in the SI counterpart under the launch condition with a small spot size and low divergent angle beam realized with an SMF probe. In general, optical transmitters for high-speed multimode data links need to realize a RML condition for MMFs. The RML condition has already been standardized using the EF in IEC. For the RML, a small-spot and low-NA beam should be created with lenses, so the launch condition for the waveguides discussed in this paper was not chosen only to evaluate the insertion loss but is also a desirable condition for high-speed multimode fiber/waveguide links.

Table 1. Insertion loss of the waveguides.

	SI waveguide	**GI waveguide**
Tx side	2.12 dB	1.99 dB
Rx side	3.11 dB	2.19 dB
Total	5.23 dB	4.18 dB
Difference between SI & GI	1.05 dB	

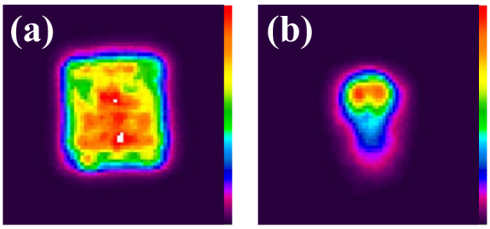

Fig. 7. NFP at connection point 2 of (a) the SI waveguide (b) the GI waveguide.

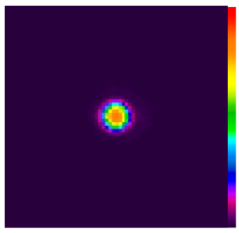

Fig. 8. NFP of single-mode fiber (SMF).

4.3 Misalignment tolerance

Figure 9 shows the misalignment tolerance curves in the direction of the X-axis at connection points 1 to 4, and Table 2 summarizes the −0.5-dB tolerance width calculated from the tolerance curves. It is noted that at all the connection points, the tolerance curves of the GI waveguide are wider than those of the SI waveguide. The reason for such wide tolerance curves in the GI waveguide is discussed below.

At connection points 1 and 3 (at the input ends of the waveguides), in general, the large core size allows higher coupling efficiency particularly under misaligned conditions. Although the originally designed core size of the SI and GI waveguides in this paper is the same (40 × 40 μm), the actual core size of the GI waveguide is measured to be slightly larger than the SI counterpart. From analyzing the NFP under the over-filled launch condition of both waveguides, it is estimated that the height of the GI core could be 5 μm larger than those of the SI core. Therefore, the GI waveguide exhibits wider tolerance curves than the SI waveguide at the input sides. If the core size were completely the same between the SI and GI, such a wider tolerance would not be observed in the GI core.

#255734 Received 14 Dec 2015; revised 30 Jan 2016; accepted 1 Feb 2016; published 11 Feb 2016

At connection points 2 and 4 (at the output sides), the coupling efficiency is largely influenced by the output spot size from the waveguide. In the case of GI waveguides, the output field size remains small due to the tight optical field confinement of the GI-core. Hence, a high coupling efficiency is obtained with the detection probes despite the different outer core shapes (square and circle). Particularly, at connection point 2, the GI waveguide shows the largest misalignment tolerance width, a 10-μm advantage over the SI waveguide, as shown in Fig. 9(b). Meanwhile, in the case of the SI waveguides, the core size directly affects their coupling efficiency with the detection probes. As mentioned above, the output NFP of the SI core waveguide at connection point 2 is spread around the outer core shape as shown in Fig. 7(a). Therefore, there is a trade-off in the core size of SI waveguides: if the core size is small, the loss at the output side (connection points 2 and 4) decreases because of the small output NFP compared to the core size of MMF and the photodetector size, while the loss at the input side (connection points 1 and 3) increases. On the contrary, in the case of GI waveguides, even if the core size is slightly larger, high coupling efficiency is realized at both input and output sides.

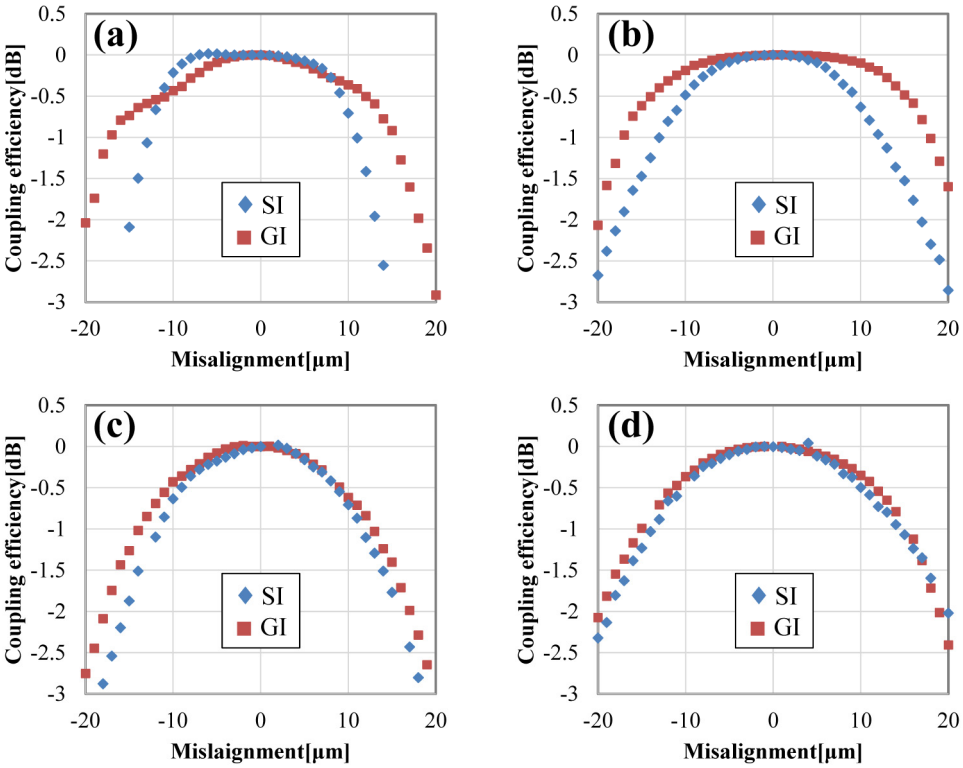

Fig. 9. Misalignment tolerance at connection point (a) 1 (b) 2 (c) 3 (d) 4.

Table 2. –0.5-dB tolerance width.

	Connection 1	Connection 2	Connection 3	Connection 4
SI waveguide	20.6 μm	19.3 μm	17.7 μm	20.2 μm
GI waveguide	22.8 μm	29.1 μm	19.6 μm	23.0 μm

5. Simulation

In order to confirm the low optical loss in the GI waveguides with 45-degree mirrors in more detail, we theoretically calculate the optical loss in the waveguide-based links using a ray-

#255734 Received 14 Dec 2015; revised 30 Jan 2016; accepted 1 Feb 2016; published 11 Feb 2016

trace simulator. For the analysis, a commercially available ray-trace simulation software, *Zemax*, is used.

5.1 Simulation model

The optical link model for the simulation is shown in Fig. 10. We focus on the optical link composed of two waveguides integrated on different O-PCBs as shown in Fig. 2. The light from a light source (spot size = 10 μm, NA = 0.20) is coupled to the waveguide on the Tx side via a 45-degree mirror. The ray power distribution is defined to have a Gaussian profile with respect to both the emission angle and the radius. The air gap between the light source and the top of the cladding is set to be 1 μm. After propagating through a 50GI-MMF, the light passes through the waveguide on the Rx side and is reflected at the mirror to be coupled to a 50-μmø photodetector.

Here, the waveguides are assumed to have a square-shaped core with a size of 40 × 40 μm based on the waveguides fabricated using the photo-addressing method mentioned above. The refractive indices of the core and the cladding are set to be 1.553 and 1.536, respectively. The cladding thickness (defined as the distance between the top of the cladding and the top of the core) is set to be 40 μm. The results of a GI waveguide are compared to those of an SI waveguide. Two index exponents (*p*, *q* parameter [15]) of the GI waveguide is set to be $p = q = 3$ because it has already been found that using the photo-addressing method, the refractive index profile with an index exponent of 3 to 4 is formed [16].

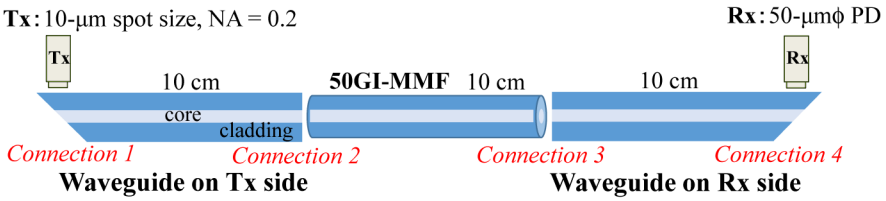

Fig. 10. Link model for simulation.

5.2 Output NFP from waveguides

Using *Zemax*, light intensity distributions can be calculated at desired positions in the link model shown in Fig. 10 by virtually placing a detector. The light intensity distributions of the output NFPs from the waveguides at connection points 2 and 4 are calculated and the results are shown in Fig. 11. The detectors are supposed to have a 40 × 40 μm square and 50-μmø circular shape at connection points 2 and 4 respectively. It is obvious that remarkably small output NFP is observed at both connection points 2 and 4 in the GI waveguide, while in the case of the SI waveguide, the light intensity distribution is uniform at both output ends.

At connection point 2, a small output NFP from the GI-core is also observed experimentally as shown in Fig. 7(b).

Furthermore, it should be noted that in the NFP at connection point 4 the light remains confined tightly at the core center in the GI waveguide, although the rays are reflected by the mirror and even propagate through the 40-μm thick cladding. Contrastingly, the NFP from the SI waveguide at connection point 4 is uniform and its size expands to a 40 × 40 μm during the propagation in the cladding. Since the size of photodiodes for high speed signals could be as small as 50-μm or less, such a wide-spread NFP causes a high coupling loss with the photodiode. Hence, we can say that GI waveguides are advantageous for O-PCB applications.

#255734 Received 14 Dec 2015; revised 30 Jan 2016; accepted 1 Feb 2016; published 11 Feb 2016

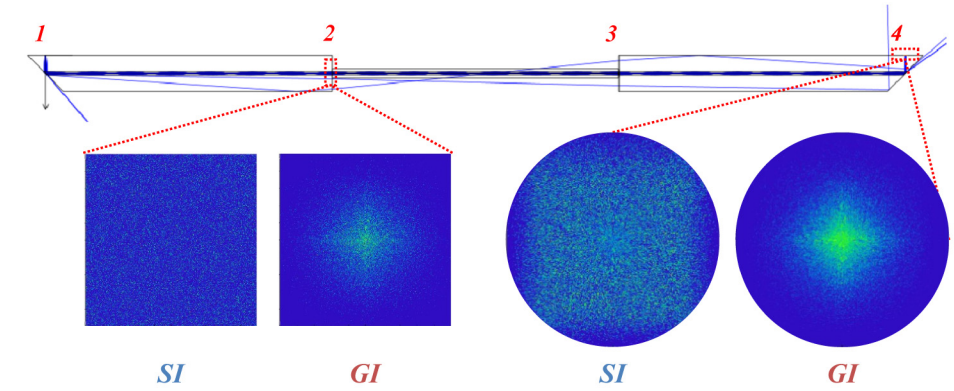

Fig. 11. Light intensity distribution at connection point 2 and 4. The detected areas of NFPs for connection points 2 and 4 are 40 × 40 μm square and 50-μmø circular shapes, respectively.

5.3 Optical link loss

In order to quantitatively analyze the link loss in the above models, optical power at connection points 2, 3, and 4 is calculated individually. Here, the core and cladding materials are assumed to exhibit no optical loss: absorption and scattering losses. Therefore, the difference of the optical power among those connection points is identical to the coupling loss at each corresponding connection point.

Figure 12 shows the total optical link loss and its breakdown into coupling loss at each connection point. The GI waveguide shows 0.57-dB total link loss: 0.74-dB advantage is observed compared to the SI waveguide which shows 1.31-dB total link loss. The GI waveguide shows remarkably lower coupling loss than SI counterpart at connection point 2. This superiority of the GI waveguide is attributed to high coupling efficiency with 50GI-MMF because of the small output NFP from the waveguide at connection point 2 as shown in Fig. 11. Contrastingly, Fig. 12 also shows that the coupling loss at connection points 3 and 4 of the GI waveguide is lower than those of the SI waveguide, which also stems from the tightly confined optical field at connection point 4 as shown in Fig. 11.

Thus, we can say that the low loss of GI waveguides (observed in both measurement and calculation) results from high coupling efficiency at the output side of the waveguides because of the optical confinement effect of the GI-core.

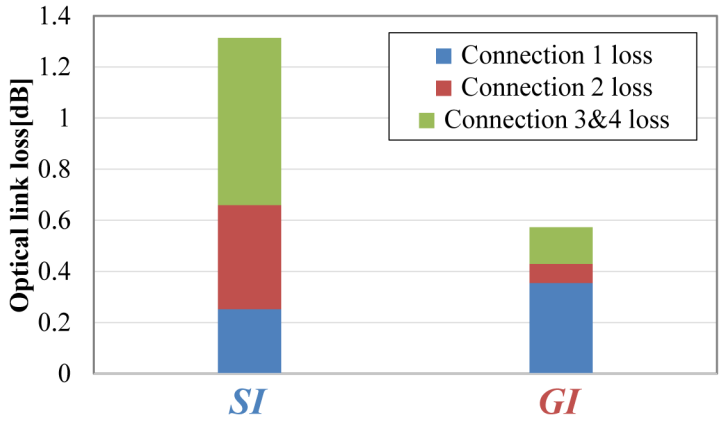

Fig. 12. Breakdown of the optical link loss.

#255734 Received 14 Dec 2015; revised 30 Jan 2016; accepted 1 Feb 2016; published 11 Feb 2016

Here, the experimentally measured absolute loss values (shown in Table 1) are higher than the theoretically simulated values. We focus on the disagreement of the loss values. As mentioned above, the calculated link loss includes no optical losses inherent to the waveguide itself in addition to Fresnel reflection loss. Therefore, the calculated optical link loss expresses only the coupling loss at connection points 1 to 4 as shown in Fig. 10, resulting in showing a very small loss values. In order to overcome this shortfall, we add the calculated propagation and Fresnel reflection losses to the simulated results.

For the propagation losses of the SI- and GI-core waveguides, we adopt the values of 0.044 dB/cm and 0.035 dB/cm, respectively. These were experimentally measured using the cut-back method. Since the waveguide used in the measurement has a length of 10 cm, the propagation loss of the SI and GI waveguides are calculated to be 0.44 dB and 0.35 dB, respectively.

Meanwhile, the Fresnel reflection loss should be observed at the boundary between the air and the cores of waveguide and fiber. Here, the loss value depends on the polarization direction and the incidence angle, but when the incident angle is zero, the reflectivity due to the Fresnel reflection, R is independent of the polarization direction, and is simply expressed as follows

$$R = \left(\frac{n_1 - n_2}{n_1 + n_2} \right)^2 \tag{1}$$

where, n_1 and n_2 are the refractive indexes of the media of incident and emitting sides, respectively. In the optical link discussed in this paper, Fresnel reflection loss could be caused at 6 points, as shown in Fig. 13. At the connection points between the light source and the waveguide, and between the waveguide and PD, air gaps (n = 1.0) should exist. Meanwhile, even at the connection points between the waveguide and fiber, Fresnel reflection loss could be caused because we do not use a matching oil at the connections. For these connection points, the Fresnel reflection losses calculated using Eq. (1) is the minimum value because the light is assumed to be injected with 0-degree of incident angle (not diverging). Table 3 shows the calculated Fresnel reflection loss at each point.

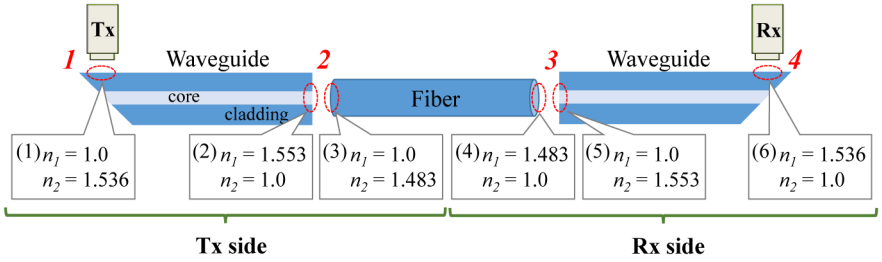

Fig. 13. Points where Fresnel reflection loss occurs.

Table 3. Calculated Fresnel reflection loss at each point.

(1)	(2)	(3)	(4)	(5)	(6)
0.198 dB	0.209 dB	0.168 dB	0.168 dB	0.209 dB	0.198 dB

Using these calculated results, the propagation loss, coupling loss, and Fresnel reflection loss at the Tx and Rx side are compared in Fig. 14. Table 4 summarizes the calculated loss at the Tx and Rx sides, where the losses are classified into three loss factors: mirror and Fresnel reflection, propagation, and connection losses. Table 4 also shows the difference in total optical loss between the SI and GI waveguides.

Table 4 shows that the GI waveguide theoretically exhibits 0.95-dB advantage over the SI waveguide, agreeing well with the measurement results of 1.05-dB advantage shown in Table

#255734 Received 14 Dec 2015; revised 30 Jan 2016; accepted 1 Feb 2016; published 11 Feb 2016

1. Thus, we confirm that the difference in the loss values between measured and calculated are mainly due to the Fresnel loss and the propagation loss of the waveguide. However, both at the Tx and Rx sides, the calculated optical loss is larger than the measured values: at the Tx side, the measured losses of the SI and GI waveguides are slightly larger than theoretical values by 0.43 dB and 0.63 dB, respectively, while at the Rx side, the SI and GI waveguides show 1.40-dB and 1.10-dB lower optical loss in the simulation than in the measurement, respectively. One of the reasons for this difference could be because the optical loss due to 45° mirrors influenced by the mirror structure: the mirror surface roughness and the mirror angle. In the simulation, no surface roughness on the mirror surface is assumed, and the mirror angle is set to be precisely 45°. Therefore, there is no loss increment due to the light scattering on rough mirror surface and angle deviation, resulting in the lower calculated optical loss at both the Tx and Rx sides in the simulation. Furthermore, for the Rx side, we used an SI-MMF for the detection probe at connection point 4 in the measurement, so the light with an NA larger than 0.33, the NA of the SI-MMF could not be coupled to the probe, although the photodetector in the simulation would receive all the light.

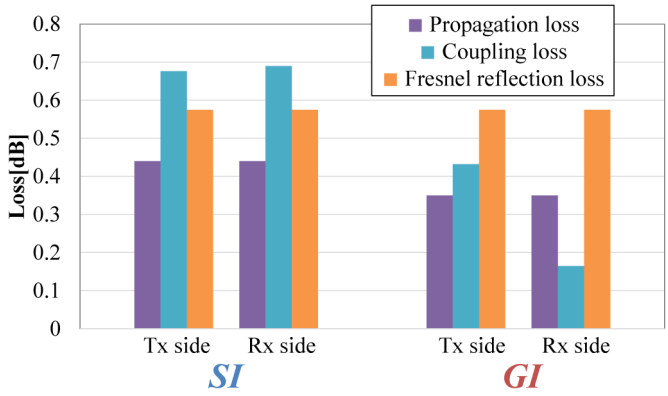

Fig. 14. Calculated optical loss.

Table 4. Calculated link loss of the waveguides.

	SI waveguide		GI waveguide	
Tx side	Mirror + Fresnel	0.47 dB	Mirror + Fresnel	0.55 dB
	Propagation	0.44 dB	Propagation	0.35 dB
	MMF connection + Fresnel	0.78 dB	MMF connection + Fresnel	0.45 dB
	Total	1.69 dB	Total	1.36 dB
Rx side	Mirror + Fresnel	0.89 dB	Mirror + Fresnel	0.36 dB
	Propagation	0.44 dB	Propagation	0.35 dB
	MMF connection + Fresnel	0.38 dB	MMF connection + Fresnel	0.38 dB
	Total	1.71 dB	Total	1.09 dB
Total	3.40 dB		2.45 dB	
Difference between SI & GI	0.95 dB			

6. Conclusion

We experimentally and theoretically investigated the optical loss at 45-degree mirrors of square-core multimode polymer optical waveguides which are assumed to be integrated on O-PCBs. It is revealed that GI-core waveguides can realize low-loss light coupling even if they are inserted in an optical link which also includes optical path conversion by 45-degree mirrors.

#255734 Received 14 Dec 2015; revised 30 Jan 2016; accepted 1 Feb 2016; published 11 Feb 2016

Acknowledgments

The authors would like to acknowledge K. Moriya of Sumitomo Bakelite Co., Ltd. for supplying the GI square-core polymer optical waveguide sample with 45-degree mirror on its one end, in addition to valuable technical advices.

#255734 Received 14 Dec 2015; revised 30 Jan 2016; accepted 1 Feb 2016; published 11 Feb 2016